Journal of Power Sources 247 (2014) 264–272

Contents lists available at ScienceDirect

Journal of Power Sources

journal homepage: www.elsevier.com/locate/jpowsour

Stabilization of the cubic perovskite in the system $La_{1-x}Ba_xCo_{1-y}Fe_yO_{3-\delta}$ ($0.7 \leq x \leq 0.9$) and its electrochemical performance as cathode materials for intermediate-temperature solid oxide fuel cells

C. Setevich [a], F. Prado [a,*], D.Z. de Florio [b], A. Caneiro [c]

[a] Depto. de Física – UNS, IFISUR – CONICET, Av. L.N. Alem 1253, 8000 Bahía Blanca, Argentina
[b] Universidade Federal do ABC, Santo André, SP 09210-170, Brazil
[c] Centro Atómico Bariloche, CNEA, Av. Bustillo 9500, 8400 S. C. de Bariloche, Argentina

HIGHLIGHTS

- The crystal structure stability and the electrochemical response of the cubic perovskites $La_{1-x}Ba_xCo_{1-y}Fe_yO_{3-\delta}$ ($0.7 \leq x \leq 0.9$) has been studied.
- Fe content needed for long term stability has been determined.
- The electrode polarization resistance was studied as a function of T, pO_2 and time.

ARTICLE INFO

Article history:
Received 18 June 2013
Received in revised form
15 August 2013
Accepted 25 August 2013
Available online 3 September 2013

Keywords:
Oxide mixed conductors
LBCF
BCFN
Phase relationship
Thermal expansion
Impedance spectroscopy

ABSTRACT

The effects of the substitution of Co by Fe on the crystal chemistry and electrode reaction of the system $La_{1-x}Ba_xCo_{1-y}Fe_yO_{3-\delta}$ ($0.7 \leq x \leq 0.9$), are investigated. The incorporation of Fe stabilizes the cubic perovskite and suppresses the structural transformation of $La_{1-x}Ba_xCoO_{3-\delta}$ from a metastable cubic perovskite to a hexagonal phase below 900 °C. The linear expansion decreases with the replacement of Co by Fe. The lowest expansion coefficient value, $\alpha \sim 20.5 \times 10^{-6}\,K^{-1}$, was obtained for the samples with Fe content $y = 0.6$. AC impedance spectroscopy measurements on symmetrical cells reveal the presence of an intermediate (IF) and a low (LF) frequency contributions at $T \geq 600$ °C. The LF arc varies with the pO_2, at 700 °C, according to a power law with exponent $n = -1$, indicating oxygen diffusion through the porous of the electrode. The minimum Rp value (0.6 Ω cm^2 at 600°C) was obtained for $La_{0.3}Ba_{0.7}Co_{0.6}Fe_{0.4}O_{3-\delta}$. At constant temperature, $T = 750$ °C, only the IF contribution varies at a rate of $3 \times 10^{-4}\,\Omega\,cm^2\,h^{-1}$, while the LF contribution remains constant. Experimental data suggest the growth of the IF arc is caused by the mismatch in the expansion coefficients of the electrode and electrolyte.

1. Introduction

Mixed conductor properties of perovskite oxides with Co in the B site have been intensely investigated as cathode material for intermediate temperature solid oxide fuel cell (IT-SOFC) since high oxide ion conductivity values were reported by Teraoka et al. [1,2] in the system $(La,Sr)(Fe,Co)O_{3-\delta}$ and particularly for $SrCo_{0.8}Fe_{0.2}O_{3-\delta}$ ($\sigma_i \sim 1$ S cm^{-1}) [2]. This compound exhibits large oxygen non-stoichiometry to charge compensate the cation Sr^{2+} in the A site, which is important to increase the oxide ionic conductivity. However, it is also responsible for the crystal structure transformation from the cubic perovskite to the brownmillerite phase $Sr_2Co_{1.6}Fe_{0.4}O_{2.5}$ with orthorhombic symmetry due to the electrostatic interaction between oxygen vacancies [3–5]. The substitution of half Sr^{2+} by the larger alkaline earth Ba^{2+}, obtaining the compound $Ba_{0.5}Sr_{0.5}Co_{0.8}Fe_{0.2}O_{3-\delta}$ (BSCF), was found to improve both the stability of the cubic perovskite phase and the oxygen permeability at high temperatures [6,7]. Furthermore, Shao and Haile [8] have reported excellent performance of BSCF as cathode material for IT-SOFC. However, recent studies [9–11] have shown that the cubic crystal structure of $Ba_xSr_{1-x}Co_{0.8}Fe_{0.2}O_{3-\delta}$ compounds are metastable transforming to a mixture of the cubic and a hexagonal phase when annealed at temperatures below

* Corresponding author. Tel.: +54 291 4595168; fax: +54 291 4595142.
E-mail addresses: fernando.prado@uns.edu.ar, fprado2007@gmail.com (F. Prado).

0378-7753/$ – see front matter © 2013 Elsevier B.V. All rights reserved.
http://dx.doi.org/10.1016/j.jpowsour.2013.08.091

900 °C during several days. More recently, the incorporation of a low concentration of Nb in the B site has been explored in order to stabilize the cubic phase in the Ba(Co,Fe,Nb)$O_{3-\delta}$ system [12,13]. It was reported the compound $BaCo_{0.7}Fe_{0.2}Nb_{0.1}O_{3-\delta}$ (BCFN) exhibits good stability under reducing atmospheres [12], and high oxygen permeation flux values [12,14]. On the other hand, the mixed conductor properties of double perovskites $LnBaCo_2O_{5+\delta}$ (Ln = La, Nd, Pr, Sm, Gd, Y) have also attracted much attention as potential candidates for cathode IT-SOFC [15–18]. In particular, the cubic perovskite phase of the series, $LaBaCo_2O_{5+\delta}$ (LBCO), with the biggest rare earth cation in the A site, La^{3+}, exhibits the highest values of power density [17] and oxygen permeability [18]. These results suggest that the incorporation of Ba^{2+} in the A site improves the performance of the mixed conductor oxides used as IT-SOFC cathode or dense ceramic separation membrane, as long as the cubic perovskite is preserved. Recently, we have studied the phase relationship and electrode polarization resistance of the composition line $La_{1-x}Ba_xCoO_{3-\delta}$ with emphasis in the Ba content range $0.5 \leq x \leq 1.0$ [19]. The cubic perovskite was obtained for the furnace cooled samples with $0.5 \leq x \leq 0.7$. For the $x = 0.6$ and 0.7, the cubic perovskites have shown to be metastable in air below $T = 1000$ °C transforming to a mixture of the cubic perovskite with a hexagonal phase, similarly to the behavior observed for $Ba_xSr_{1-x}Co_{0.8}Fe_{0.2}O_{3-\delta}$ [9–11]. Samples with $x = 0.8$ and 0.9 resulted in a mixture of phases with a predominant hexagonal phase. In spite of this, very low polarization resistance values, $R_p \sim 0.065$–$0.075\ \Omega\ cm^2$ at 600 °C, were obtained for samples with $0.5 \leq x \leq 0.7$ using a graded cathode [19,20].

With an aim to stabilize the cubic perovskite phase in the $La_{1-x}Ba_xCoO_{3-\delta}$ system, for the Ba content range $0.7 \leq x \leq 0.9$, we explored the substitution of Co by Fe. In this paper we have determined the composition range for which the cubic phase stabilizes and the effects of Fe doping on the crystal structure, thermal expansion, and electrode polarization resistance of the cubic $La_{1-x}Ba_xCo_{1-y}Fe_yO_{3-\delta}$ phases.

2. Experimental

$La_{1-x}Ba_xCo_{1-y}Fe_yO_{3-\delta}$ with $0.7 \leq x \leq 0.9$ and $0.1 \leq y \leq 0.6$, $Ba_{0.5}Sr_{0.5}Co_{0.8}Fe_{0.2}O_{3-\delta}$ (BSCF) and $BaCo_{0.7}Fe_{0.2}Nb_{0.1}O_{3-\delta}$ (BCFN) compounds were synthesized by a conventional solid-state reaction technique. Required amounts of La_2O_3, previously dried overnight at 1000 °C, in air, $BaCO_3$, $SrCO_3$, Fe_2O_3, Nb_2O_5 and Co_3O_4 were mixed and ground with a mortar and pestle and heat treated at 850 °C for 8 h in air. Subsequently, the powders were ball milled during 1 h using an agate milling media, pressed into pellets and sintered at temperatures ranging between 1100 and 1150 °C for 12 h, in air. Afterward the samples were cooled at a rate of 1 °C min^{-1} to room temperature. The oxygen content of those samples with cubic crystal structure was determined by iodometric titration [21]. Measurements were repeated three times for each sample, in order to estimate the error of the data.

X-ray diffraction (XRD) data were collected at room temperature with a Philips PW1700 diffractometer using Cu Kα radiation and a graphite monochromator from $2\theta = 10$–80° with a counting time of 1 s per 0.02°. The crystal structures of the samples were analyzed by the Rietveld method using the FullProf Program [22].

The linear expansions of the $La_{1-x}Ba_xCo_{1-y}Fe_yO_{3-\delta}$ compounds were measured on cylindrical samples of approximately 5.0 mm diameter and 4–5 mm height, from room temperature to 900 °C, using a LINSEIS L75PT Series dilatometer. All the samples were heated up to 900 °C at 5 °C min^{-1}, and, after a 1 h dwell were cooled to room temperature at a rate of 1 °C min^{-1}. They were then once again heated to 900 °C at a rate of 1C min^{-1}, in air. Experimental data were corrected using Al_2O_3 as a standard.

The polarization resistance of the $La_{1-x}Ba_xCo_{1-y}Fe_yO_{3-\delta}$ electrodes, in air, was studied by impedance spectroscopy measurements on electrochemical cells using GDC as electrolyte and a symmetrical configuration. Commercial $Ce_{0.9}Gd_{0.1}O_{1.95}$ powder from Praxair Specialty Ceramics was pressed into 12.5 mm diameter disks, applying a uniaxial pressure of 500 kg cm^{-2}, and calcined at 1350 °C during 4 h, in air. After sintering, the electrolyte disks were approximately 9.8 mm in diameter and around 0.5 mm thick. Both sides of the electrolytes were cleaned with solvent before spraying the electrodes. The inks for electrode deposition were prepared mixing the corresponding ceramic powders with ethanol, α-terpineol, polyvinyl butyral, and polyvinyl pyrridone in appropriate ratio. To eliminate adherence problems to the electrolyte a porous GDC layer was sprayed on the dense electrolyte, and then the cell was heat treated at 1300 °C during 1 h. Subsequently, the pure $La_{1-x}Ba_xCo_{1-y}Fe_yO_{3-\delta}$ layer was sprayed onto the porous GDC layer, the assemblage was heat treated at 1000 °C for 1 h, in air.

The impedance spectroscopy measurements were performed at temperatures in the range $400 \leq T \leq 750$ °C, in flowing air of 200 ml min^{-1}, by steps of 50 °C. The data acquisition was performed by an Autolab system PGSTAT-30 coupled to a module FRA2 in a frequency range of 1 MHz and 10^{-3} Hz. An AC signal of 50 mV was applied to the cell, under zero DC polarization. Gold grids, slightly pressed on the porous electrodes using a mullite tube, were used as current collectors. Impedance diagrams were analyzed using Z-view2 software [23].

The microstructure and thickness of the porous layers and interfaces were characterized by scanning electron microscopy (SEM) using a Philips 515 microscope.

3. Results and discussion

The phase relationship in $La_{1-x}Ba_xCo_{1-y}Fe_yO_{3-\delta}$ samples with high Ba content ($x = 0.7$, 0.8 and 0.9) and Fe content in the range $0.1 \leq y \leq 0.6$ was studied by XRD. The powder XRD patterns were obtained after the samples were heat treated at 1100–1150 °C, in air, during 12 h and cooled at the rate of 1 °C min^{-1} to room temperature. For the samples $La_{0.3}Ba_{0.7}Co_{1-y}Fe_yO_{3-\delta}$ with Ba content $x = 0.7$ and Fe content in the range $0.1 \leq y \leq 0.6$, the XRD patterns were indexed according to the cubic perovskite phase (SG P*m*-3*m*). In the case of $La_{0.2}Ba_{0.8}Co_{1-y}Fe_yO_{3-\delta}$, the XRD pattern for the sample with Fe content $y = 0.1$ reproduces the one obtained for the sample with pure Co in the B site ($y = 0$) in our previous work [19]. The peak reflections correspond to a mixture of phases consisting of the cubic perovskite and a hexagonal phase, most likely the 12H (SG P 63/*mmc*) [24], which was identified in our previous work after a heat treatment of 8 days at $T = 850$ °C [19]. On the other hand, the XRD patterns of the samples with Fe content $y \geq 0.2$ were indexed according to the crystal structure of the cubic perovskite and no reflections belonging to secondary phases were detected. Similarly, for the $La_{0.1}Ba_{0.9}Co_{1-y}Fe_yO_{3-\delta}$ sample ($x = 0.9$), a mixture of phases was obtained for $y = 0.1$ and 0.2, while for $y \geq 0.3$ the patterns correspond to the cubic perovskite. For instance, Fig. 1 shows the XRD data corresponding to the line composition $La_{0.1}Ba_{0.9}Co_{1-y}Fe_yO_{3-\delta}$ with the Fe content varying from $y = 0.1$ to $y = 0.6$. In this figure, we plot the square root of the intensity in order to eventually magnify low intensity reflections from secondary phases.

In order to check the stability of the cubic phases obtained with the substitution of Co by Fe, those samples whose crystal structure resulted cubic were heat treated in air at 750 °C during 10 days. The obtained XRD data for the angle range $20 \leq 2\theta \leq 50°$ are displayed in Fig. 2 along with the XRD patterns corresponding to the compounds BSCF and BCFN heat treated using similar conditions. Fig. 2a

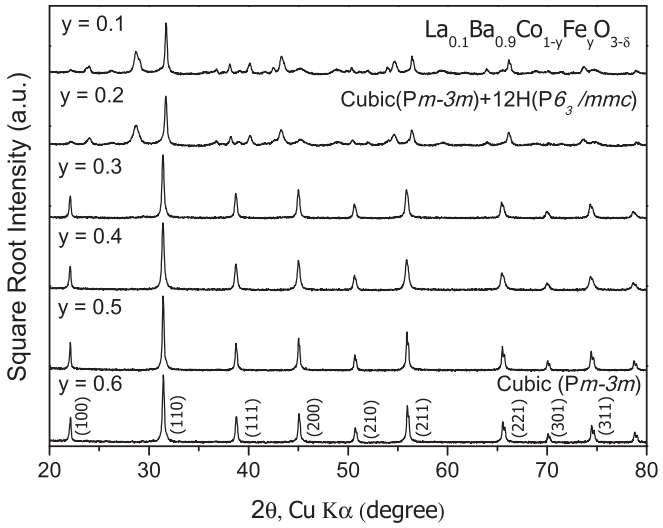

Fig. 1. XRD patterns of $La_{0.9}Ba_{0.1}Co_{1-y}Fe_yO_{3-\delta}$ samples with $0.1 \leq y \leq 0.6$ after the synthesis heat treatment at 1100–1150 °C.

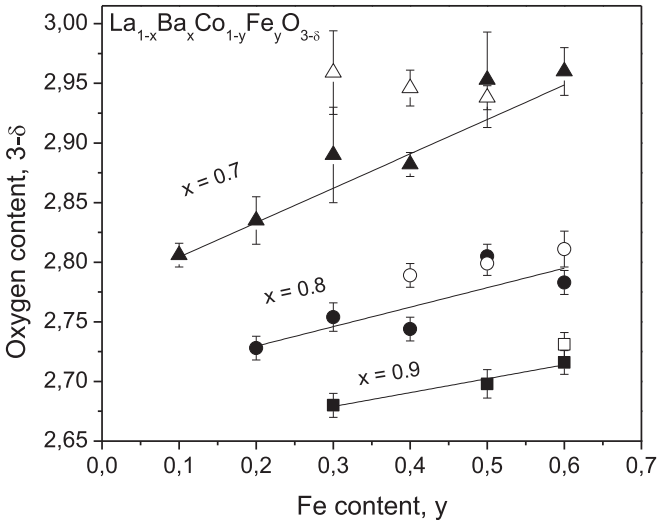

Fig. 3. Oxygen content $(3 - \delta)$ as a function of Ba and Fe content for $La_{1-x}Ba_xCo_{1-y}Fe_yO_{3-\delta}$ samples with the cubic perovskite crystal structure. Solid symbols correspond to samples cooled at 1 °C min^{-1} while open symbols correspond to the samples annealed at 750 °C during 10 days.

shows the XRD diffraction data for BSCF. In agreement with previous reports [9,11], the cubic phase is metastable transforming to a mixture of the cubic perovskite with the 2H hexagonal phase. Unexpectedly, we have found that the material BCFN containing Nb, which has been proposed recently for high temperature electrochemical applications [12–14,25] is also unstable during long term heat treatments at $T = 750$ °C. Fig. 2b clearly shows the presence of reflections indicating the formation of secondary phases in BCFN. Fig. 2c–f shows the XRD patterns for $La_{0.1}Ba_{0.9}Co_{1-y}Fe_yO_{3-\delta}$ samples with $0.3 \leq y \leq 0.6$. In this case, only the $y = 0.6$ sample remains single phase with the cubic perovskite crystal structure. As the Ba content decreases from 0.9 to 0.7, the Fe content needed to avoid the formation of secondary phases at $T = 750$ °C decreases to $y = 0.4$ for $x = 0.8$ and $y = 0.3$ for $x = 0.7$ (see Fig. 2g–k).

The oxygen content $(3 - \delta)$ of the single cubic perovskite phases in the system $La_{1-x}Ba_xCo_{1-y}Fe_yO_{3-\delta}$ was determined at room temperature by iodometric titration. Fig. 3 shows the variation of the oxygen content as a function of the Ba and the Fe content. Solid symbols correspond to the cubic perovskite phases cooled at a rate of 1 °C min^{-1}, while open symbols correspond to cubic perovskites annealed at $T = 750$ °C during 10 days. As the Ba content increases from $x = 0.7$ to $x = 0.9$, the oxygen content of the samples for a given Fe content decreases to charge compensate the higher content of Ba^{2+}. On the other hand, as the Fe content increase, so does the oxygen content, indicating the stabilization of higher oxidation states of Fe is easier than in the case of Co. The average oxidation state of (Fe, Co) calculated from charge neutrality and the oxygen

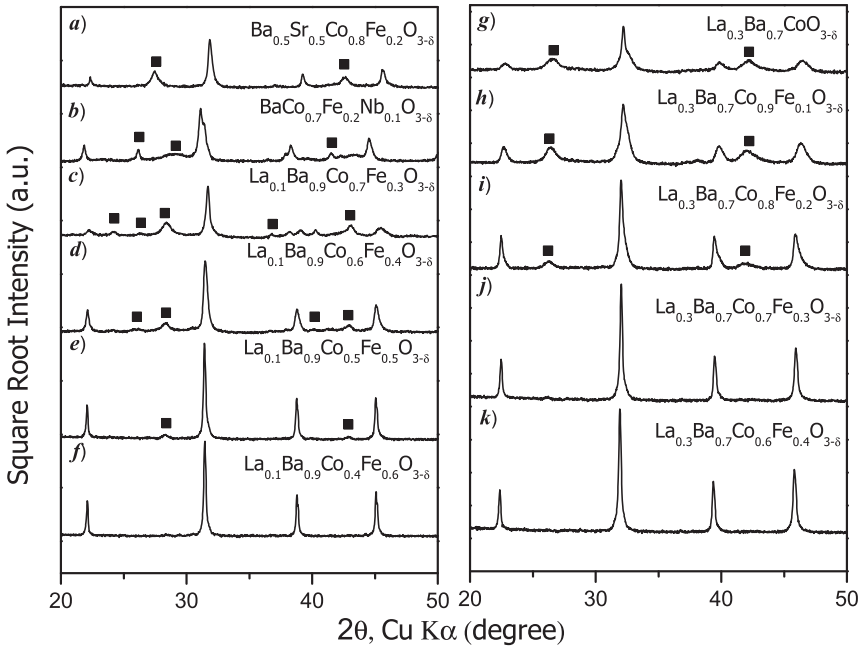

Fig. 2. XRD patterns of $La_{1-x}Ba_xCo_{1-y}Fe_yO_{3-\delta}$ samples after the heat treatment at 750 °C, in air, during 10 days. a) BSCF; b) BCFN; c–f) $x = 0.9$ and $y = 0.3$, 0.4, 0.5 and 0.6 and g–k) $x = 0.7$ and $y = 0.0$, 0.1, 0.2, 0.3 and 0.4. Solid squares indicate the reflections of secondary phases.

content values determined by iodometric titration, always gives values above 3+ for all these samples. Finally, the oxygen content values of the samples annealed at 750 °C during 10 days are always somewhat higher than those obtained for the samples cooled at 1 °C min^{-1}.

The formation of crystal structures with different symmetry (hexagonal, cubic, orthorhombic, tetragonal or rhombohedral) for the ABO_3 compounds is usually explained with the Goldschmidt's tolerance factor given by the equation:

$$t = \frac{r_A + r_O}{\sqrt{2}(r_B + r_O)}$$

where r_A, r_B and r_O are the ionic radii tabulated by Shannon [26] for the cations A, B and oxide ions, respectively. Fig. 4 shows the variation of the tolerance factor with the Fe content for $La_{1-x}Ba_xCo_{1-y}Fe_yO_{3-\delta}$. The tolerance factor was calculated approximating the Co and Fe oxidation states by 3+ and 4+ with high spin configuration, respectively. This approximation is consistent with the oxygen content values displayed in Fig. 3, the charge neutrality relation and the fact that Fe oxidation states are higher than the Co oxidation states. Solid symbols represent those samples formed by a mixture of phases after the initial heat treatment at 1100–1150 °C, while empty symbols indicates metastable samples, initially with a cubic structure, which then transforms to a mixture of phases as a consequence of the long term heat treatment at 750 °C. Finally half filled symbols show those compositions with the cubic perovskite crystal structure after the long term heat treatment at 750 °C. In Fig. 4, the experimental data for the samples with $x = 0.5$ and 0.6 and $y = 0$, obtained in a previous work [19], and the data for $BaCoO_{3-\delta}$ and BCFN are also included. In this way the range of the tolerance factor where the cubic perovskite phases of the $La_{1-x}Ba_xCo_{1-y}Fe_yO_{3-\delta}$ system are stable, according to XRD data, is clearly revealed and the boundary of this region increases with the Fe content.

The variation of the cubic perovskite lattice parameter a with the Fe content is shown in Fig. 5. While for the $x = 0.9$ samples, the lattice parameter clearly decreases with the substitution of Co by Fe, for $x = 0.8$ this behavior is less evident and for $x = 0.7$ the lattice parameter remains almost constant. Finally, the lattice parameter increases with the Ba content. The diminution of the lattice parameter a with the substitution of Co for Fe was already reported for the perovskite phases $Ba_{0.5}Sr_{0.5}Co_{1-y}Fe_yO_{3-\delta}$ with $0 \le y \le 1.0$ [27] and $BaCo_{1-y}Fe_yNb_{0.2}O_{3-\delta}$ with $0 \le y \le 0.8$ [14]. In these perovskite phases, the incorporation of Fe^{3+} replacing $Co^{+2/+3}$ cations reduces the oxygen vacancy concentration, which is compensated by raising the Co oxidation state towards +3 [14], thus decreasing the ionic radii of the Co cations [26] and consequently the lattice parameters. In the case of the $La_{1-x}Ba_xCo_{1-y}Fe_yO_{3-\delta}$ samples, the average oxidation state of (Fe,Co) is above 3+. If we assume that the majority fraction of Fe cations is 4+, charge neutrality indicates the majority fraction of Co cations is 3+. Therefore, the incorporation of Fe^{4+} with smaller ionic radii than Co^{3+} [26] would explain the reduction of the lattice parameter with the increase of the Fe content. Fig. 5 also reveals that the lattice parameter obtained for the samples heat treated at 1100–1150 °C are systematically higher than those obtained for the samples heat treated during 10 days at 750 °C. This behavior can be explained considering that samples heat treated at 750 °C systematically display larger oxygen content values, which reduces the cubic perovskite lattice parameter.

The volume expansion of the $La_{1-x}Ba_xCo_{1-y}Fe_yO_{3-\delta}$ compounds with cubic crystal structure was studied in the temperature range $40 \le T \le 900$ °C, in air, through linear expansion measurements. Fig. 6 shows the $\Delta L/L_0$ vs. T curves for these samples during a cooling/heating run. ΔL represents the sample length change and L_0 the length of the sample at the temperature of reference $T = 40$ °C. The linear expansion $\Delta L/L_0$ increases with the raise of temperature. During heating, the slope of the $\Delta L/L_0$ vs. T curves clearly increases after the temperature range of $350 \le T \le 400$ °C. This is due to oxygen atoms being removed from the crystal structure, which is known as chemical expansion [28,29]. Thus, at low temperatures the thermal expansion is the only contribution to the linear expansion, while at high temperature both the chemical and the thermal expansions are significant which causes an increment in the slope of the $\Delta L/L_0$ vs. T curves. During the cooling/heating run the presence of hysteresis was detected mainly around the temperature value where the slope of the $\Delta L/L_0$ vs. T curves increases. This effect is associated to the cooling/heating rate (1 °C min^{-1}), which is not slow enough to assure the equilibrium at each temperature [19]. In Table 1 the expansion coefficient values $\alpha = \Delta L/(L_0\,\Delta T)$ obtained for the two temperature ranges $40 \le T \le 300$ and $450 \le T \le 900$ °C are listed. While the substitution of Co by Fe

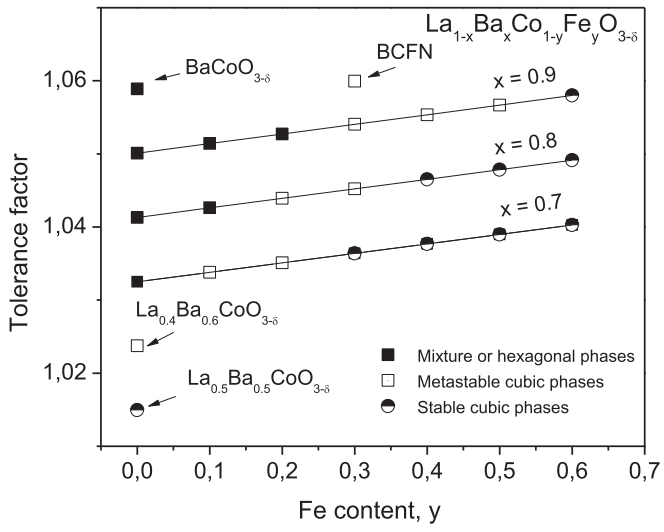

Fig. 4. Variations of the tolerance factor t as a function of the Fe and Ba content for $La_{1-x}Ba_xCo_{1-y}Fe_yO_{3-\delta}$ samples. ■) solid squares indicate the compositions formed by a mixture of phases after the heat treatment at 1100–1150 °C; □) open squares indicate single cubic phases that transform to a mixture of phases after the heat treatment at 750 °C during 10 days; ◓) Stable cubic phases after the heat treatment at 750 °C during 10 days.

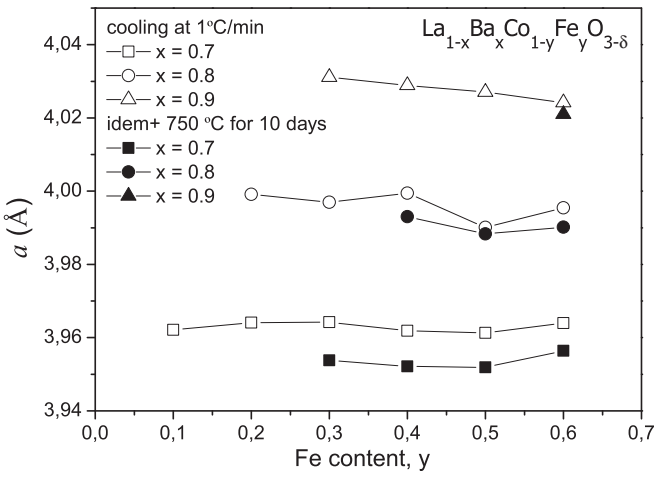

Fig. 5. Variations of the lattice parameter a as a function of the Fe and Ba content for the cubic perovskite phases.

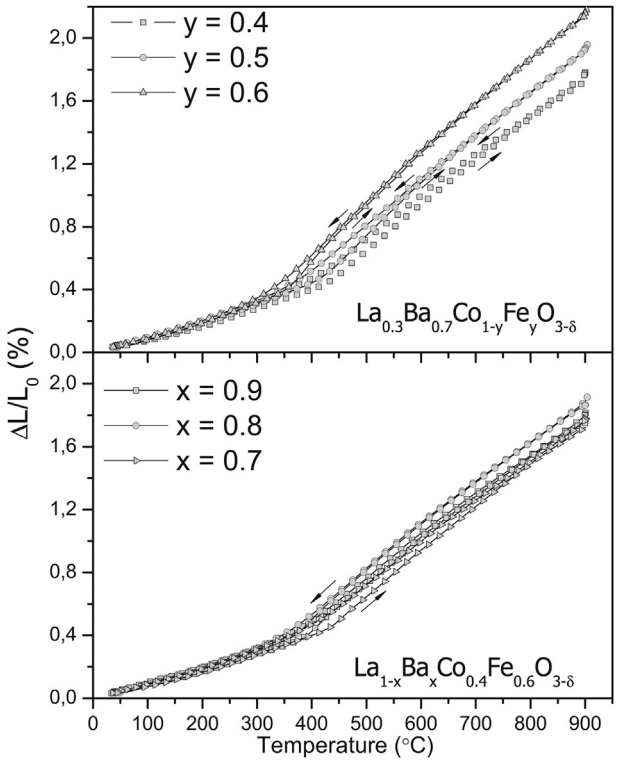

Fig. 6. Relative length change $\Delta L/L_0$ as a function of temperature for cubic phases of the $La_{1-x}Ba_xCo_{1-y}Fe_yO_{3-\delta}$ system. a) Samples with $x = 0.3$ and $y = 0.4$, 0.5 and 0.6; and b) samples with $x = 0.7$, 0.8 and 0.9 and $y = 0.6$.

clearly reduces the volume expansion of the samples in the whole temperature range, the replacement of La by Ba lead to little variations on the expansion coefficient with no clear trend. As we have discussed above, the substitution of Co by Fe reduces the oxygen vacancy concentration, and therefore the chemical expansion contribution, to charge compensate the raise of the transition metals oxidation state. At low temperature the α values varies between 10×10^{-6} and 12×10^{-6} K^{-1}, while at high temperature it varies from 26.5 to 30.4×10^{-6} K^{-1} resulting in average values between 20.3×10^{-6} K^{-1} for $La_{0.3}Ba_{0.7}Co_{0.4}Fe_{0.6}O_{3-\delta}$ and 24.7×10^{-6} K^{-1} for $La_{0.3}Ba_{0.7}Co_{0.6}Fe_{0.4}O_{3-\delta}$.

The electrode polarization resistances of $La_{1-x}Ba_xCo_{1-y}Fe_yO_{3-\delta}$ phases with stable cubic crystal structure were studied by means of impedance spectroscopy measurements in the temperature range $450 \leq T \leq 750$ °C, in air, using symmetrical cells. The electrodes deposited on dense GDC pellets consisted of two layers: one of porous GDC, approximately 5 μm thick, on the surface of the electrolyte to avoid adherences issues [19,20] and a porous layer of the perovskite phases $La_{1-x}Ba_xCo_{1-y}Fe_yO_{3-\delta}$ 30 μm thick. For instance, Fig. 7 shows a SEM micrograph of the electrode cross section of a cell prepared with the cubic perovskite

Table 1
Expansion coefficient values for $La_{1-x}Ba_xCo_{1-y}Fe_yO_{3-\delta}$ samples.

Samples	Expansion coefficient (10^{-6} K^{-1})		
	40–300 °C	450–900 °C	40–900 °C
$La_{0.3}Ba_{0.7}Co_{0.6}Fe_{0.4}O_{3-\delta}$	12.05	30.41	24.7
$La_{0.3}Ba_{0.7}Co_{0.5}Fe_{0.5}O_{3-\delta}$	10.96	29.17	22.0
$La_{0.3}Ba_{0.7}Co_{0.4}Fe_{0.6}O_{3-\delta}$	10.16	27.6	20.3
$La_{0.2}Ba_{0.8}Co_{0.4}Fe_{0.6}O_{3-\delta}$	10.83	27.07	21.6
$La_{0.1}Ba_{0.9}Co_{0.4}Fe_{0.6}O_{3-\delta}$	10.14	26.53	20.5

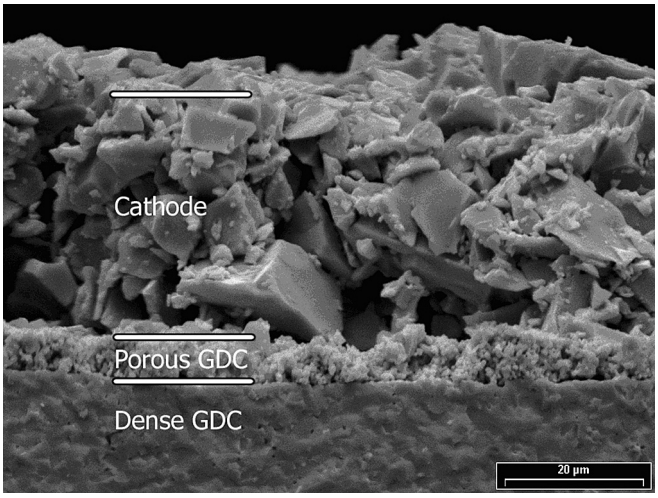

Fig. 7. SEM micrograph of the electrode cross-section prepared with $La_{0.3}Ba_{0.7}Co_{0.6}Fe_{0.4}O_{3-\delta}$.

$La_{0.3}Ba_{0.7}Co_{0.6}Fe_{0.4}O_{3-\delta}$. The image of the cathode reveals the presence of ceramic grains of sizes in the 5–10 μm range. During the sample preparation good adhesion and connectivity between the electrode and the electrolyte were observed.

The behavior of the impedance data in the temperature range $450 \leq T \leq 750$ °C, in air, was found to be similar for all the electrode materials tested. Fig. 8 shows the variation of the impedance spectra with temperature for the $La_{0.3}Ba_{0.7}Co_{0.6}Fe_{0.4}O_{3-\delta}$ electrode. Systematically, the impedance of the symmetrical cell becomes positive at high frequency denoting an inductive contribution from the device and leads. The impedance data reveal the presence of three impedance arcs in the Nyquist plane each associated to a different process. At low temperature, $T = 450$ °C, two impedance arcs are observed, a broad arc at the low frequency limit, labeled intermediate frequency (IF) arc, and a small arc at the high frequency region (HF). As the temperature increases, the polarization resistance associated to the IF arc decreases and the apex frequency moves towards higher values overlying the HF arc, which becomes negligible. A third arc (LF) clearly appears on the low frequency side, however, it is not detected at low temperatures, where it is negligible with respect to the IF contribution. In addition, R_{LF} polarization resistance shows little variation with temperature. Based on these observations the impedance diagrams were reproduced with an equivalent circuit consisting of a pure resistance in series with an inductance in parallel with a resistance and three elements (R_i, CPE) formed by a resistance R_i in parallel with a constant phase element $CPE = 1/(B(j\omega)^p)$; where B is a constant and p a parameter that may vary from $p = 1$ for a pure capacitor, to $p = -1$ for a pure inductance (see Fig. 8).

We will now discuss the contributions to the polarization resistance observed for these electrodes with emphasis on the IF and LF mechanisms. The analysis of the experimental data obtained in air shows that the capacitance values of the IF arcs varies between 4×10^{-3} and 7×10^{-2} F cm^{-2} depending of the chemical composition, but it shows little variation with temperature for a given composition. Also, the apex frequency of the IF arc increases with temperature from $\sim 10^{-1}$ Hz at 450 °C to $\sim 1.5 \times 10^3$ Hz at 750 °C indicating the relaxation time of this process is thermally activated. Fig. 9 shows the Arrhenius plot of the intermediate frequency polarization resistance, R_{IF}, for all the electrode materials. The calculated activation energy values fluctuate between 1.0 and 1.25 eV with no clear trend. On the other hand, the polarization resistance R_{LF} and the apex frequency of the LF arc remain almost

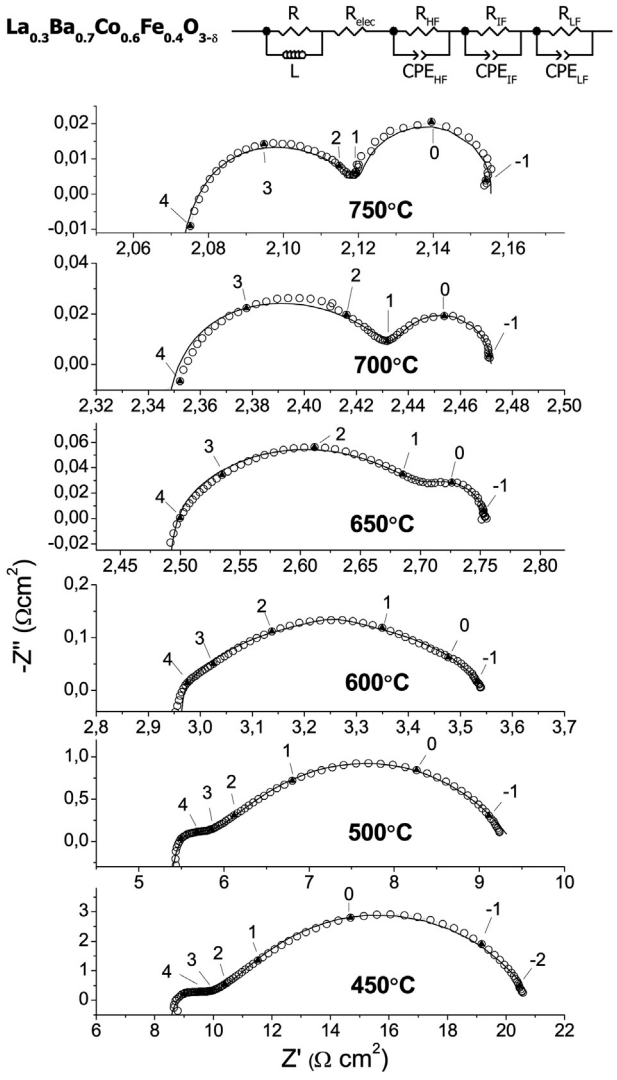

Fig. 8. Variations of the impedance diagram with temperature, in air, for $La_{0.3}Ba_{0.7}Co_{0.6}Fe_{0.4}O_{3-\delta}$. The solid line corresponds to the fit of the experimental data using the equivalent circuit displayed at the top of the figure. The logarithm of the frequency is indicated in the figure.

unchanged at $\sim$0.04 Ω cm^2 and 1 Hz, respectively, indicating that the chemical composition mainly affects the IF arc. Fig. 10 shows the impedance spectra at constant temperature, $T = 700$ °C, for electrode materials with different composition. It can be seen that the shape of the impedance diagrams is similar for all the electrodes. Noteworthy, the size of the LF arc remains almost constant, while the polarization resistance of the IF arc tend to increase as either the Fe or Ba content increases. This behavior confirms that the rate-limiting mechanism corresponding to the IF arc is affected by the chemical composition of the electrode. For instance, this could be any one involving the electrode material as oxygen adsorption, charge transfer at the gas/electrode interface, oxide ion bulk or surface diffusion, charge transfer at the electrode/electrolyte interface [30].

The variation of the impedance spectra with the oxygen partial pressure was determined at 700 °C for all the electrodes in the range $6.5 \times 10^{-4} \leq pO_2 \leq 1$ atm. For instance, Fig. 11 exhibits the evolution of the impedance diagrams for the $La_{0.3}Ba_{0.7}Co_{0.6}Fe_{0.4}O_{3-\delta}$ electrode. The Z' values of the spectra were modified in such a way that the intersection of the experimental data with the x-axis occurs at $Z' = 0$. The impedance diagram under

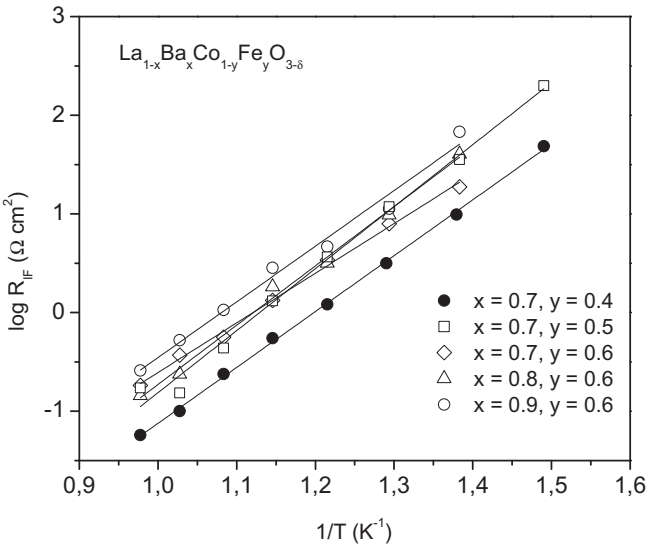

Fig. 9. Arrhenius plot of the polarization resistance, R_{IF}, associated to the intermediate frequency contribution for $La_{1-x}Ba_xCo_{1-y}Fe_yO_{3-\delta}$ electrode materials, in air.

pure oxygen ($pO_2 = 1$ atm) consists of only one arc. As soon as the pO_2 decreases, a second arc at the low frequency side is revealed. This behavior is consistent with the lack of an oxygen concentration gradient in the porous electrode under a pure oxygen atmosphere and consequently of the gas phase diffusion contribution to the polarization resistance of the electrode [31]. After further

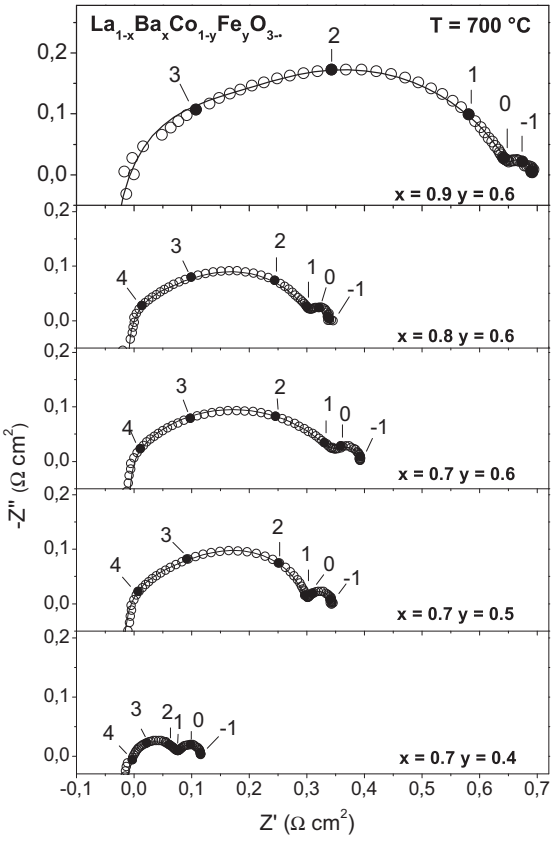

Fig. 10. Complex impedance spectra of $La_{1-x}Ba_xCo_{1-y}Fe_yO_{3-\delta}$ electrodes at 700 °C, in air. The logarithm of the frequency is indicated in the figure.

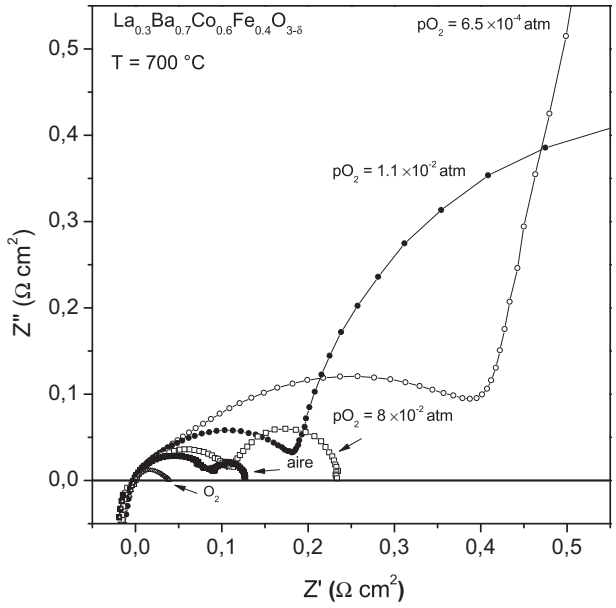

Fig. 11. Variations of the impedance diagrams with the pO_2 at 700 °C for $La_{0.3}Ba_{0.7}Co_{0.6}Fe_{0.4}O_{3-\delta}$.

decreasing the pO_2, both impedance arcs increase their size. Fig. 12 shows the dependence of the IF and LF polarization resistances with the pO_2 for $La_{0.3}Ba_{0.7}Co_{0.6}Fe_{0.4}O_{3-\delta}$, which is a typical behavior for these material electrodes. Usually, the log (R) vs. log (pO_2/atm) plots are analyzed using the power law:

$$R = C \times (pO_2)^n$$

where C is a constant and n an exponent related with the limiting step of the electrode polarization [32–34]. For the low frequency polarization resistance (R_{LF}), the linear fit of the experimental data yield a slope value of $n \sim -1$, which is consistent with a rate-limiting process controlled by the oxygen gas phase diffusion in the porous phase of the electrode [30,34,35]. This conclusion is also

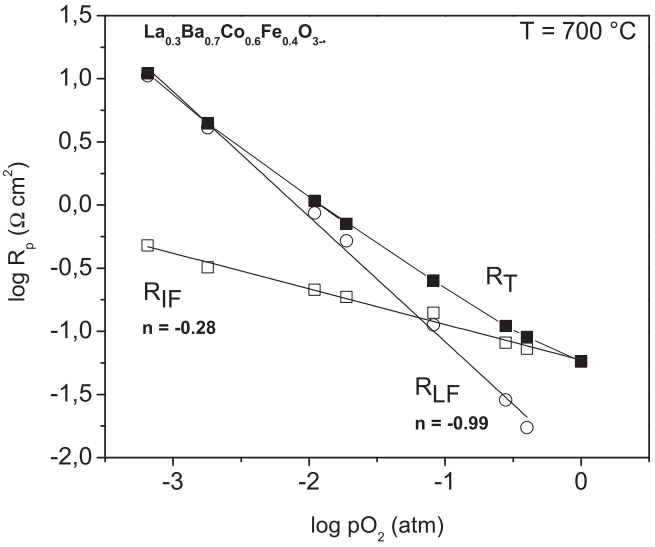

Fig. 12. Variation of the polarization resistance for $La_{0.3}Ba_{0.7}Co_{0.6}Fe_{0.4}O_{3-\delta}$ with the oxygen partial pressure (pO_2). The log R_{IF} vs. log (pO_2) and log R_{LF} vs. log (pO_2) plots are also included.

supported by the capacitance values ranging between 1.4 and 6 F cm^{-2} and the weak dependence on temperature of the LF impedance arc expected for this contribution [36,37]. Regarding the IF polarization resistance, it increases as the pO_2 decreases. The dependence of R_{IF} with the pO_2, revealed by the negative value of the exponent $n \sim -0.28$, is opposite to the variation reported in the perovskite $La_{0.6}Sr_{0.4}Co_{0.8}Fe_{0.2}O_{3-\delta}$ [34] for which the polarization resistance is controlled by the oxide ion diffusion in the crystal lattice, suggesting this is not the main rate mechanism controlling the IF polarization resistance. An exponent value n close to −0.25 has been assigned to different mechanisms such as a convoluted process involving adsorption and surface exchange [38] or surface diffusion of oxygen intermediate species [39]. However, a more detailed work is needed in order to determine the controlling mechanism for this contribution to the polarization resistance of these perovskites.

The variation of the total polarization resistance with time while the cell is at constant temperature, $T = 750$ °C, or after it is cycled in the temperature range $400 \leq T \leq 750$ °C is shown in Fig. 13 for the $La_{0.3}Ba_{0.7}Co_{0.6}Fe_{0.4}O_{3-\delta}$ electrode. The profile temperature during impedance measurements is displayed in Fig. 13a. The cell was kept at constant temperature, $T = 750$ °C, during approximately 160 h, it was then cycled two times between 750 °C and 400 °C. Fig. 13b shows the variation of the total polarization resistance of the electrode with time and the contribution of the IF and LF processes to the total R_p. Impedance data shows that the total polarization resistance increases with time at a rate of 3×10^{-4} Ω cm^2 h^{-1}. Noteworthy the low frequency arc shows no variation indicating that the microstructure of the electrode remains unchanged with time. On the contrary, the contribution of the IF process to the polarization resistance systematically increases. After a period of 160 h, the cell was cycled two times between $400 \leq T \leq 750$ °C. Once again, impedance data show that the total polarization resistance increases after each cycle (see points B and C in Fig. 13b) due to the IF process. Fig. 13c shows the impedance spectra corresponding to times t = 0, 50 and 155 h and after the last temperature cycle where a continuous broadening of the IF arc is clearly observed. This behavior, usually observed in cobaltites [40], suggests the increase of R_p with time and after temperature cycling could be related to a continuous degradation of the electrode/electrolyte interface due to the mismatch in the expansion coefficients of these materials.

Finally, Fig. 14 shows the Arrhenius plot of the total polarization resistance (R_p) obtained for the $La_{1-x}Ba_xCo_{1-y}Fe_yO_{3-\delta}$ electrodes, in air. It can be observed that the incorporation of Fe increases the polarization resistance of the electrode materials compared to the values (~0.13 Ω cm^2 at 600 °C) obtained in a previous paper [20] for Fe free electrodes with a cell configuration similar to the one used in this work. From all the compositions tested, the minimum polarization resistance was obtained for the $La_{0.3}Ba_{0.7}Co_{0.6}Fe_{0.4}O_{3-\delta}$ material.

4. Conclusions

The effects of the substitution of Co by Fe on the crystal structure stability and electrochemical behavior as cathode materials for IT-SOFC of the system $La_{1-x}Ba_xCo_{1-y}Fe_yO_{3-\delta}$ for $0.7 \leq x \leq 0.9$, have been studied. It was found that the replacement of Co by Fe stabilizes the cubic perovskite phase in the $La_{1-x}Ba_xCoO_{3-\delta}$ system. The Fe content needed to stabilize the cubic perovskite phase increases from $y = 0.3$ to $y = 0.6$ as the Ba content increases from $x = 0.7$ to $x = 0.9$. The total expansion (thermal and chemical) of the stable cubic perovskite phases decreases with the replacement of Co by Fe from 24.7×10^{-6} K^{-1} for $La_{0.3}Ba_{0.7}Co_{0.6}Fe_{0.4}O_{3-\delta}$ to 20.3×10^{-6} K^{-1} for $La_{0.3}Ba_{0.7}Co_{0.4}Fe_{0.6}O_{3-\delta}$. Impedance

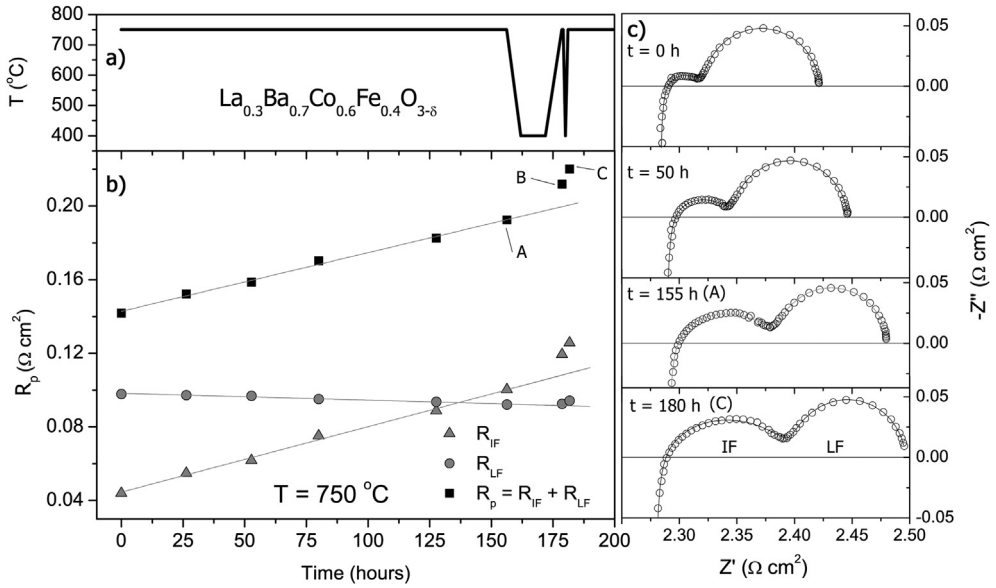

Fig. 13. Time dependence of the polarization resistance for the electrode prepared with the cubic phase $La_{0.3}Ba_{0.7}Co_{0.6}Fe_{0.4}O_{3-\delta}$. a) Temperature profile used during measurements; b) R_p vs. t, R_{IF} vs. t and R_{LF} vs. t plots. Points B and C indicates the polarization resistance after each temperature cycle; c) complex impedance spectra at $t = 0$, 50, 155 h and after the two temperature cycles. The solid lines correspond to the fit of the experimental data using the equivalent circuit included at the top of Fig. 8.

spectroscopy measurements reveal three contributions to the electrode polarization resistance, however only the contributions at intermediate (IF) and low (LF) frequency are relevant at $T \geq 600$ °C. The LF polarization resistance varies with the pO_2, at 700 °C, according to a power law with an exponent $n = -1$, which is expected for oxygen diffusion through the porous of the electrode. The minimum polarization resistance ($R_p = 0.6\ \Omega\ cm^2$ at 600 °C) was obtained for $La_{0.3}Ba_{0.7}Co_{0.6}Fe_{0.4}O_{3-\delta}$. For this electrode, the polarization resistance slowly increases as a function of time at a rate of $3 \times 10^{-4}\ \Omega\ cm^2\ h^{-1}$ at $T = 750$ °C. The raise of R_p is caused by an increment of the IF contribution (R_{IF}), while the LF contribution (R_{LF}) remains constant with time. This behavior was also observed after carrying out two temperature cycles thus suggesting the increment of R_p, and therefore of R_{IF}, is associated to a continuous deterioration of the electrode/electrolyte interface due to the mismatch in the expansion coefficients of the electrode and electrolyte. In summary, we think the identification of the stable cubic perovskite phases in the system $La_{1-x}Ba_xCo_{1-y}Fe_yO_{3-\delta}$ and the experimental information on its electrochemical properties may help to design a better cathode material for IT-SOFC.

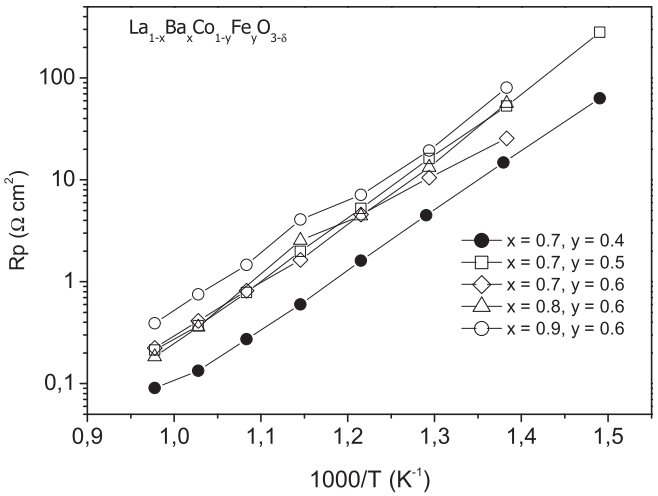

Fig. 14. Arrhenius plot of the total polarization resistance, R_p, for $La_{1-x}Ba_xCo_{1-y}Fe_yO_{3-\delta}$ electrode materials in air.

Acknowledgments

This work was supported by CNEA (Argentine Atomic Energy Commission), ANPCyT, Argentina, through PICT 2008-00102 and 2010-0322 and SPU (Argentina) and CAPES (Brazil) through PFPG 011/2011.

References

[1] Y. Teraoka, H.M. Zhang, S. Furukawa, N. Yamazoe, Chem. Lett. (1985) 1743–1746.
[2] Y. Teraoka, H.M. Zhang, K. Okamoto, N. Yamazoe, Mater. Res. Bull. 23 (1988) 51–58.
[3] L.M. Liu, T.H. Lee, L. Qiu, Y.L. Yang, A.J. Jacobson, Mater. Res. Bull. 31 (1996) 29–35.
[4] N. Grunbaum, L. Mogni, F. Prado, A. Caneiro, J. Solid State Chem. 177 (2004) 2350–2357.
[5] F. Prado, N. Grunbaum, A. Caneiro, A. Manthiram, Solid State Ionics 167 (1–2) (2004) 147–154.
[6] Z. Shao, W. Yang, Y. Cong, H. Dong, J. Tong, G. Xiong, J. Membr. Sci. 172 (2000) 177–188.
[7] Z. Shao, H. Dong, G. Xiong, Y. Cong, W. Yang, J. Membr. Sci. 183 (2001) 181–192.
[8] Z. Shao, S.M. Haile, Nature 431 (2004) 170–173.
[9] S. Švarcová, K. Wiik, J. Tolchard, H. Bouwmeester, Tor Grande, Solid State Ionics 178 (2008) 1787–1791.
[10] Z. Yáng, J. Martynczuk, K. Efimov, A.S. Harvey, A. Infortuna, P. Kocher, L.J. Gauckler, Chem. Mater. 23 (2011) 3169–3175.
[11] M. Arnold, T. Gesing, J. Martynczuk, A. Feldhoff, Chem. Mater. 20 (2008) 5851–5858.
[12] Y. Cheng, H. Zhao, D. Teng, F. Li, X. Lu, W. Ding, J. Membr. Sci. 322 (2008) 484–490.
[13] C. Zhu, X. Liu, C. Yi, L. Pei, D. Yan, J. Niu, D. Wang, W. Su, Electrochem. Commun. 11 (2009) 958–961.
[14] J. Yi, J. Brendt, M. Schroeder, M. Martin, J. Membr. Sci. 387–388 (2012) 17–23.
[15] A.A. Taskin, A.N. Lavrov, Y. Ando, Appl. Phys. Lett. 86 (2005) 091910:1–091910:3.
[16] A. Tarancón, S.J. Skinner, R.J. Chater, F. Hernández-Ramírez, J. Kilner, J. Mater. Chem. 17 (2007) 3175–3181.
[17] J.-H. .Kim, A. Manthiram, J. Electrochem. Soc. 155 (2008) B385–B390.
[18] J.-H. Kim, L. Mogni, F. Prado, A. Caneiro, J.A. Alonso, A. Manthiram, J. Electrochem. Soc. 156 (2009) B1376–B1382.
[19] C. Setevich, L. Mogni, A. Caneiro, F. Prado, J. Electrochem. Soc. 159 (2012) B73–B80.
[20] C. Setevich, L. Mogni, A. Caneiro, F. Prado, Int. J. Hydrogen Energy 37 (2012) 14895–14901.
[21] A. Manthiram, S. Swinnea, Z.T. Sui, H. Steinfink, J.B. Goodenough, J. Am. Chem. Soc. 109 (1987) 6667–6669.

[22] J. Rodríguez-Carvajal, Fullprof: a program for Rietveld Refinement and Profile Matching Analysis of Complex Powder Diffraction Patterns, Laboratoire Léon Brillouin (CEA-CNRS).
[23] D. Johnson, Zview Version 2.9b. Copyright, Scribner Associates, Inc., 1990–2005.
[24] A.J. Jacobson, J.L. Hutchinson, J. Solid State Chem. 35 (1980) 334–340.
[25] Zhi-Bin Yang, Min-Fang Han, P. Zhu, F. Zhao, F. Chen, Int. J. Hydrogen Energy 36 (2011) 9162–9168.
[26] R.D. Shannon, Acta Crystallogr. A 32 (1976) 751–767.
[27] Z. Chen, R. Ran, W. Zhou, Z. Shao, S. Liu, Electrochim. Acta 52 (2007) 7343–7351.
[28] S.B. Adler, J. Am. Ceram. Soc. 84 (2001) 2117–2119.
[29] S. McIntosh, J.F. Vente, W.G. Haije, D.H.A. Blank, H.J.M. Bouwmeester, Chem. Mater. 18 (2006) 2187–2193.
[30] C. Deportes, M. Duclot, P. Fabry, J. Fouletier, A. Hammou, M. Kleitz, E. Siebert, J.L. Souquet, Electrochimie des Solides, Presses Universitaires de Grenoble, Grenoble, 1994.
[31] K. Huang, J. Electrochem. Soc. 151 (2004) H117–H121.
[32] Y. Takeda, R. Kanno, M. Noda, Y. Tomoda, O. Yamamoto, J. Electrochem. Soc. 134 (1987) 2656–2661.
[33] A. Ringuedé, J. Fouletier, Solid State Ionics 139 (2001) 167–177.
[34] N. Grunbaum, L. Dessemond, J. Fouletier, F. Prado, L. Mogni, A. Caneiro, Solid State Ionics 180 (2009) 1448–1452.
[35] L. Mogni, N. Grunbaum, F. Prado, A. Caneiro, J. Electrochem. Soc. 158 (2011) B202–B207.
[36] H. Gu, H. Chen, L. Gao, L. Guo, Electrochim. Acta 54 (2009) 7094–7098.
[37] R.C. Reid, J.M. Prausnitz, B.E. Poling, The Properties of Gases and Liquids, fifth ed., Mc Graw-Hill, New York, 2001 (Chapter 11).
[38] A. Esquirol, N.P. Brandon, J.A. Kilner, M. Mogensen, J. Electrochem. Soc. 151 (2004) A1847–A1855.
[39] X.J. Chen, K.A. Khor, S.H. Chan, J. Power Sources 123 (2003) 17–25.
[40] J. Xie, Young-Wan Ju, T. Sakai, T. Ishihara, J. Solid State Electrochem. 17 (2013) 2251–2258.